



# Surface hydrographic and water mass variability in the eastern equatorial Pacific during interglacial-like Marine Isotope Stage 14



Pai-Sen Yu <sup>a, c, \*</sup>, Markus Kienast <sup>b</sup>, Min-Te Chen <sup>c</sup>, Isabel Cacho <sup>d</sup>, Jos Abel Flores <sup>e</sup>

<sup>a</sup> Taiwan Ocean Research Institute, National Applied Research Laboratories, Kaohsiung, 801, Taiwan

<sup>b</sup> Department of Oceanography, Dalhousie University, Halifax, Nova Scotia, Canada

<sup>c</sup> Institute of Applied Geosciences, National Taiwan Ocean University, Keelung, 20224, Taiwan

<sup>d</sup> Department of Stratigraphy, Paleontology, and Marine Geosciences, University of Barcelona, 08028, Barcelona, Spain

<sup>e</sup> Department of Geology, University of Salamanca, 37008, Salamanca, Spain

## ARTICLE INFO

### Article history:

Received 18 November 2016

Received in revised form

20 December 2016

Accepted 20 December 2016

Available online 1 March 2017

### Keywords:

Eastern equatorial Pacific  
Marine Isotope Stage (MIS) 14  
Multiple sea surface temperature  
Eastern equatorial Pacific cold tongue  
ITCZ

## ABSTRACT

Surface temperature and water masses variability in the Eastern Equatorial Pacific (EEP) is sensitive to global climate changes in response to either Northern/Southern Hemisphere forcing or low-latitude atmosphere-ocean feedback. High-latitude processes can influence tropical oceans via atmospheric bridges and oceanic tunnels, whereas perturbations in the low-latitude atmosphere-ocean modulate the behavior of low-latitude oceans. For climate paradoxes of prolonged warmth MIS (Marine Isotope Stage) 15–13, little has known about any causes or any possible tele-connections between the EEP and high-/low-latitudes because lack of observations. To address this issue, multiple sea surface temperature (SST) records (i.e. faunal transfer function-based, Mg/Ca ratio on mono-species, and  $U^{K}_{37}$ -derived temperature estimates) and faunal-derived water masses are generated from the EEP core ODP 1240. Our results reveal a glacial EEP MIS 14 cooling ( $\sim 1\text{--}2\text{ }^{\circ}\text{C}$ ) with higher eastern boundary current faunal abundances as compared to adjacent interglacial stages. In a glacial MIS 14 scenario, we suggest that the EEP areas would receive more nutrient-rich, cold waters from high latitudes via the Peru-Chile Current. The atmospheric bridge of a northwardly Intertropical Convergence Zone (ITCZ) shift and the resulting heat/moisture transport across the eastern equatorial Atlantic (EEA) would weaken the magnitude of the EEP cold tongue in MIS 14. We also think of another scenario in that the orbital variations in glacial MIS 14 was characterized by higher obliquity fluctuations, lower eccentricity/precession. The orbital variations shape an inter-hemispheric asymmetry with higher seasonality. This scenario could result in a stagnant/inactive Atlantic Meridional Ocean Circulation and northward shifts in the ITCZ/southward displacement of westerlies in the southeastern Pacific during MIS 14. The retreat of the West Antarctic sea ice and enhancement of the Antarctic Circumpolar Current would also bring less high-latitude cold upwelled water (the Subantarctic Mode Water/Antarctic Intermediate Water) into the eastern tropical Pacific/Atlantic Oceans. We suggest that a diminished La Niña-like condition and a relatively weakened EEP/EEA cold tongue developed in glacial MIS 14 compared to other glacial MIS in the late Quaternary. The interglacial-like MIS 14 is therefore characterized by a small-magnitude of eastern tropical upwelling areas and greater extension of western Pacific/Atlantic warm surface waters. Such amplifications in glacial MIS 14 could lead to less fluctuation of Termination VI and persistent warmth in MIS 15–13.

© 2016 Elsevier Ltd and INQUA. All rights reserved.

## 1. Introduction

Orbital and continental ice volume variations (with interactive effects from changing atmospheric greenhouse gas contents) have

been widely viewed as dominant pacemakers in late Quaternary climate variability (Berger et al., 1993; Shackleton, 2000; Ruddiman, 2006). Prior to the Mid-Brunhes Transition (MBT; c.a. 500–400 ka) there are well-documented climate paradoxes, such as the long interglacial Marine Isotope Stage (MIS) 11 (e.g. Droxler et al., 2003) and the mid-Pleistocene climate transition (MPT; Mudelsee and Schulz, 1997; Raymo et al., 2004). As the Earth's orbit undergoes a relative low-amplitude ETP variation (orbital forcing including eccentricity, tilt, and precession; Berger et al., 1993;

\* Corresponding author. Taiwan Ocean Research Institute, National Applied Research Laboratories, Kaohsiung, 801, Taiwan.

E-mail address: [epson\\_yu@narlabs.org.tw](mailto:epson_yu@narlabs.org.tw) (P.-S. Yu).

Laskar et al., 2004) from the MPT to the MBT, MIS 16–11 of the coolest interglacial type in glacial MIS 14 and the strongest glacial maxima in MIS 16 (or MIS 12) are revealed by benthic oxygen isotope signatures (e.g. LR04 stack; Lisiecki and Raymo, 2005). Some of the climate paradoxes of benthic foraminiferal  $\delta^{13}\text{C}_{\text{max}}$  episodes (c.a. 500 ka; Raymo et al., 1997, 2004; Tian et al., 2002) and plateau-like planktic foraminiferal  $\delta^{18}\text{O}$  signatures during MIS 15–13 (e.g. Bassinot et al., 1994) have been addressed. However, we still do not have a clear understanding of the dynamics and impacts of climate variability during the unusually long interglacial MIS 15–13, with an interglacial-like MIS 14.

We attempt to address what are the possible mechanisms that have been responsible for the warm, interglacial-like MIS 14 expressed in particular in the Eastern Equatorial Pacific (EEP). We provide evidence that support a scenario in that an increase in the moisture of the western Pacific source regions in MIS 14 is revealed by more freshening waters and a weakening of the eolian flux (~30%) in the South China Sea (SCS) as compared with glacial MIS 2 (Clemens et al., 2008; Yu and Chen, 2011). This is in accordance with increased  $\delta^{15}\text{N}$  signatures and depleted terrestrial sediment flux off the Arabian Sea, indicating that upwelling-induced productivity and less moisture in glacial MIS 14 is in responses to the intensified Indian summer monsoon (Clemens et al., 1996; Altabet et al., 1999). At the Eastern Equatorial Atlantic (EEA) lowering of the eolian content would result from a strengthened Africa summer monsoon (Tiedemann et al., 1994). Given the close linkage to this nearly synchronous climate pattern, the warmth and humidity in monsoon-prevailing areas have been linked to stronger monsoon systems and greater heat storage in the Western Pacific Warm Pool (WPWP) interior (de Garidel-Thoron et al., 2005; Medina-Elizalde and Lea, 2005; Yu and Chen, 2011). Weaker or terminated ventilation of the Atlantic thermohaline circulation during MIS 14 can be inferred from the benthic  $\delta^{13}\text{C}$  evidence (Ruddiman et al., 1989; Raymo et al., 1997; Lisiecki and Raymo, 2005).

In the terrestrial realm, parts of the mid-latitude land environment does not seem to synchronously experience cold conditions at higher latitudes during MIS 14. Loess-paleosol sequences retrieved from the central Chinese Loess Plateau (Heslop et al., 2000; Sun et al., 2005) indicate a distinct climate transition (i.e. the most prominent paleosol S5, equivalent to MIS 15–13 intervals) characterized by increased warmth/precipitation across the mid-latitudes because of the strengthened (weakened) of the Asian summer (winter) monsoon. Anomalous warmer/wetter conditions in glacial MIS 14 have also been observed in Eurasia, as revealed by sapropel-forming in the eastern Mediterranean and greater biogenic silica content from Lake Baikal in Siberia (Rossignol-Strick and Paterne, 1999; Prokopenko et al., 2006).

Several newly developed observations have suggested that basin-wide Pacific dynamical adjustments in the tropics would shed more light on the climate paradox of the hemispheric asymmetry between the marine and terrestrial evidence during MIS 14. However, due to severe carbonate dissolution and limited high-resolution cores in the EEP, no much evidence of reconstructing surface ocean hydrographic variability of basin-wide oceans during of MIS 15–13 has been presented. Until the Ocean Drilling Program (ODP) Leg 202 cruise to the EEP (Mix et al., 2003), cores drilled from ODP Site 1240 ( $0^{\circ}1.311'N$ ,  $86^{\circ}27.758'W$ ; water depth 2921 m) provided excellent material for multiple sea surface temperature (SST) estimations by proxy data. In this study, multi-SST records are reconstructed by a faunal-based transfer function, alkenone-derived estimates, and a Mg/Ca ratio from planktic foraminifer shells using ODP 1240 cores. These SST records reflect the sensitivity of the tropical EEP and a possible interaction between the Intertropical Convergence Zone (ITCZ), EEP cold tongue, and cross-basin water vapor transports. Moreover, we further evaluate the

tropical atmosphere-ocean feedback in the EEP and how a possible EEP climatic response was affected by the slowing or even stagnation of Atlantic thermohaline circulation during MIS 15–13. In relation to the enigma of MIS 15–13, this evidence further suggests how climate conditions/thresholds would cause an interglacial-like MIS 14 scenario and might trigger the paradoxes of resultant ocean variability (e.g. the MBT formation and  $\delta^{13}\text{C}_{\text{max}}$  episodes).

## 2. Regional setting

The study site was obtained from Hole ODP 1240 ( $0^{\circ}1.311'N$ ,  $86^{\circ}27.758'W$ ; water depth 2921 m) and was retrieved from the north of the Carnegie Ridge in the Panama Basin during the ODP LEG 202 cruise (Mix et al., 2003) (Fig. 1). The Panama Basin region represents a crucial location for understanding the paleoceanographic evolution of the EEP, as it is located at the equatorial front of two modern major surface circulations, the eastward-flowing equatorial undercurrent (EUC) and the northward-propagating Peru-Chile Current (PCC). The EUC originates in the southwestern Pacific or the Southern Ocean (i.e. SAMW, the Subantarctic Mode Water), and flows eastward along the equator at a water depth of 40 m in the EEP. The eastern boundary current (EBC) PCC is characterized by cold ( $<24^{\circ}\text{C}$ ) and nutrient-rich (nitrate concentration  $>10\ \mu\text{mol/L}$ ) water and is formed by the southern Pacific-wide subtropical gyre. The global-encircling Antarctic Circumpolar Current (ACC) (Pennington et al., 2006) circulates along the South American margin and thus serves as one of the strongest EBCs (Toggweiler et al., 1991; Kessler, 2006). The seasonal ocean variations in the EEP are due to the equatorial Pacific cold tongue-ITCZ dynamics. The most dramatic feature of the EEP surface ocean occurs from early July through late October, and is associated with seasonal positions of the ITCZ. While the ITCZ shifts to its northern position from boreal summer to autumn, the EEP region undergoes

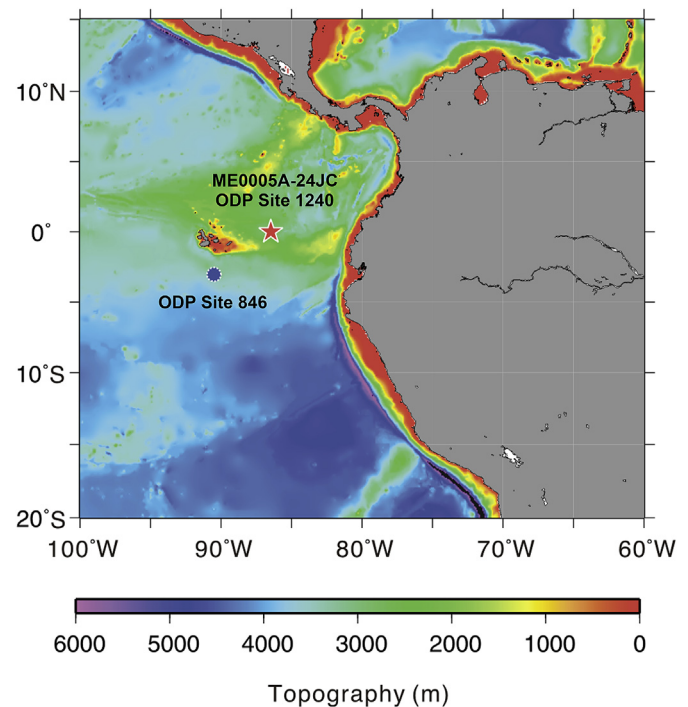


Fig. 1. ODP Site 1240 ( $0^{\circ}1.311'N$ ,  $86^{\circ}27.758'W$ ), close to core ME0005-24JC ( $0^{\circ}1.3'N$ ,  $86^{\circ}27.8'W$ ; water depth 2941 m), was retrieved at a water depth of 2921 m, north of the Carnegie Ridge in the Panama Basin in the EEP. Marine core ODP Site 846 used in this study is also shown.

a stronger prevailing southeastern trade wind. As a result, this wind-driven current causes a divergence upwelling (i.e. the Ekman divergence) along the equator, and thus generates profound tongue-like cool water in the vicinity of the EEP. Another significant feature of coastal upwelling off the Nazca Rise, which is activated by the southeastern trade wind, may contribute some nutrient-rich cold surface waters to our study areas. In contrast, as the ITCZ moves southward from early November to late January (i.e. austral late spring to the summer season), the EEP receives more warm water vapors from the EEA across the isthmus of Panama and then the prevailing northeastern trade winds further expand the oligotrophic tropical warm water of the eastern equatorial warm pool (i.e. the Panama Basin). Some warm water forms a northern equatorial countercurrent and the EUC flows southward to about 2–5°S. Thus it also inhibits advections of PCC cold waters into the Panama Basin. Indeed, this equatorial front, a striking feature of the seasonal hydrographic transition (SST and sea surface salinity; SSS), can be observed within the latitudinal migration from 5°N to 5°S (Pennington et al., 2006). The position of the equatorial front is also influenced by warm water vapors across the WEA. In addition, in terms of the zonal connection over the cross-equatorial Pacific, one impact of the ENSO fluctuations between the El Niño and La Niña phases may be to modify atmosphere-ocean conditions toward a more steady-state phase. Hydrographic conditions with high mixing of water masses at Site 1240 are dynamically constrained by ITCZ migration, the eastern equatorial Pacific cold tongue, and even by ENSO climate evolution.

### 3. Materials and methods

#### 3.1. Stable oxygen isotope analysis and chronology

The preferred *Globigerinoides ruber sensu stricto* (s.s.)/*sensu lato* (s.l.) with 250–350 µm size fraction were unavailable for either stable oxygen isotope analysis ( $\delta^{18}\text{O}$ ) at EEP downcore ODP 1240. For  $\delta^{18}\text{O}$  analysis, 5–6 specimens of surface-dwelling species *Globigerinoides sacculifer* (no sac-like final chamber) were picked from 43.16 to 63.36 m composite depth (mcd). The foraminifers with 8 cm resolution were processed using the standard procedures (see Yu et al., 2008) and the foraminiferal stable oxygen isotope measurements were carried out at the Institute of Earth Science, Academia Sinica, Taiwan. The analytical error ( $1\sigma$ ) for  $\delta^{18}\text{O}$  is better than  $\pm 0.007\%$ . Each reported  $\delta^{18}\text{O}$  data represents the average of two to three measurement runs.

The timescale calibration of the isotopic stages corresponds to a planktic foraminifer *G. ruber* stack of ODP 677 (Shackleton et al., 1990). Our age model is mainly reconstructed by oxygen isotope stratigraphy and then re-evaluated by independent chronological

methods comprised of biostratigraphic events (458 ka; nannofossil *Pseudoemiliana lacunose*) (Flores et al., 2006) and paleomagnetic data (~780 ka; the Brunhes/Matuyama polarity transition) (Mix et al., 2003) (see Table 1, Fig. 2). The planktic oxygen isotope record documents a continuous >200-ky period from MIS 16 to 12 (ca. 670–440 ka). The age of each sample is then calculated by linear interpolation between adjacent age-control points, assuming a constant sedimentation rate within the time interval (Howell, 2001).

#### 3.2. Multiple SST estimations

In order to understand the sensitivity of different temperature methodologies and the magnitude of EEP SST variability, we present multiple SST estimations reconstructed from a modified EP Imbire-Kipp transfer function (IKTF; Yu et al., 2012), an alkenone unsaturation ratio ( $U^{K'_{37}}$  index; e.g. Prahl et al., 2006), and Mg/Ca ratios on *G. ruber* s.s./s.l (e.g. Anand et al., 2002; Barker et al., 2003). (See Supplementary A). Temperature estimate errors among the IKTF-type, alkenone-based, and Mg/Ca-derived methods would be 1.8 °C, 1.0 °C and 1.0 °C, respectively. Furthermore, downcore planktic foraminifer compositions with 8-cm resolution are used to depict possible variations in the characteristics of high-resolution surface water masses in the EEP. The details for development of the regional IKTF with the EP MARGO dataset (MARGO Project Members, 2009) are reported in Yu et al. (2012).

### 4. Results

#### 4.1. SST variability

In the sediments of Site 1240, multiple temperature estimates based on the EP IKTF, alkenone index  $U^{K'_{37}}$ , and Mg/Ca ratios on *G. ruber* s.s./s.l. successfully demonstrate significant EEP mean SST fluctuations during the MIS 16–13 interval (Fig. 3b–d). The calculated mean temperature amplitude using the Mg/Ca approach shows more variation (–6 °C; 19.7–25.7 °C) than the other two indices, which are ~4 °C in magnitude for faunal- and alkenone-SSTs (22.2/22.4–26.3 °C). Yet, multi-SSTs at the MIS 15/14 or MIS 14/13 transition show low-amplitude changes with only ~1–2 °C. Calculating the contamination effect on Mg/Ca-SST, we found that major trace metals (i.e. Mn/Ca, Fe/Ca and Al/Ca) had no major correlations with Mg/Ca-SST estimates (Fig. 3d–g). These observations are also consistent with previous results on the uppermost section of Site 1240 (Pena et al., 2005). Such a contamination effect would have less bias at Site 1240. Thus a colder condition illustrated by ODP 1240 Mg/Ca SSTs could only probably because of suffering a poor carbonate preservation of foraminifer shells and/or different

**Table 1**  
Age model for ODP site 1240.

Method	Depth (cmcd)	Age (ka)	Sedimentation Rate (cmcd/kyr)	Source	
$\delta^{18}\text{O}$ : <i>G. sacculifer</i> (no sac)	4364	457	6.15	This study	
$\delta^{18}\text{O}$ : <i>G. sacculifer</i> (no sac)	4444	470	9.81		
$\delta^{18}\text{O}$ : <i>G. sacculifer</i> (no sac)	4650	491	12.33		
$\delta^{18}\text{O}$ : <i>G. sacculifer</i> (no sac)	4872	509	10.50		
$\delta^{18}\text{O}$ : <i>G. sacculifer</i> (no sac)	5019	523	4.10		
$\delta^{18}\text{O}$ : <i>G. sacculifer</i> (no sac)	5105	544	8.20		
$\delta^{18}\text{O}$ : <i>G. sacculifer</i> (no sac)	5392	579	7.50		
$\delta^{18}\text{O}$ : <i>G. sacculifer</i> (no sac)	5707	621	6.00		
$\delta^{18}\text{O}$ : <i>G. sacculifer</i> (no sac)	5743	627	7.21		
$\delta^{18}\text{O}$ : <i>G. sacculifer</i> (no sac)	5916	651	7.21		
Biostratigraphic datum					
LAD of <i>Pseudoemiliana lacunosa</i>	4366	458	8.18		Flores et al., (2006)
Paleomagnetic datum	7000	780			Mix et al., (2003)

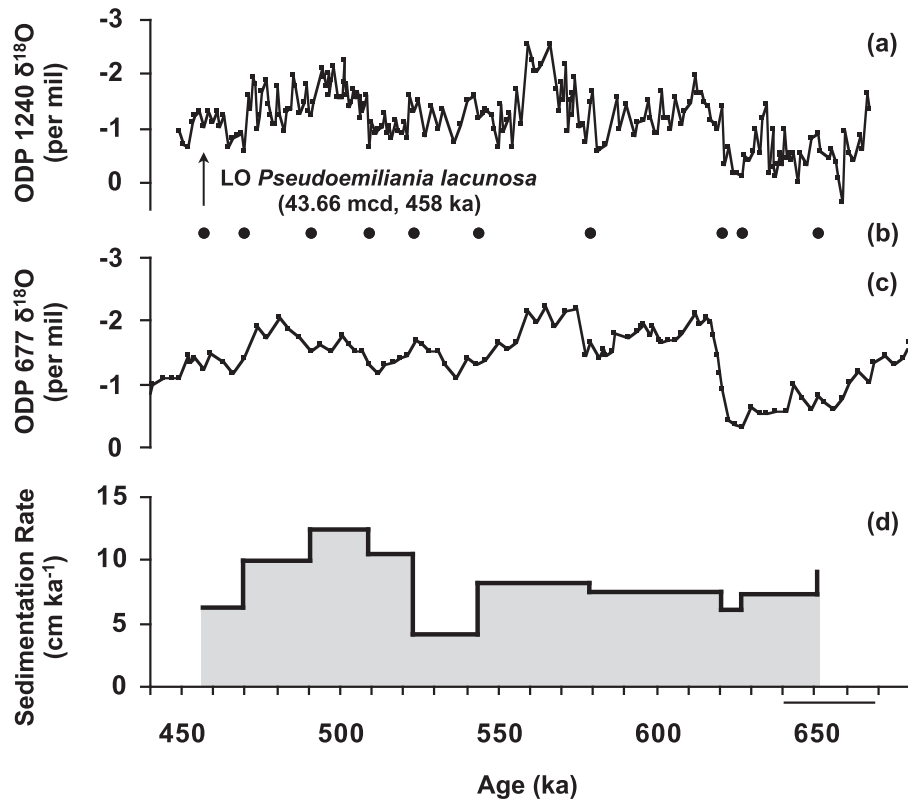


**Fig. 2.** (a) ODP Site 1240  $\delta^{18}\text{O}$  planktic foraminifer *G. sacculifer* were compared with the (b) ODP Site 677 stack, respectively. ODP Site 677 stack tie points (solid circles) were used in this stratigraphy. Our oxygen stratigraphy is in good agreement with the last appearance of the nannofossil *Pseudoemiliana lacunosa* datum (43.66 mcd, 458 ka) (Flores et al., 2006); (c) ODP Site 1240 sedimentation rate as reconstructed from age control points, indicates that high sedimentation rates ranged from 7 to 18 cm/kyr over these two time slices.

preferred habitat of water depths for *G. ruber* s.l.. However, a profound Pacific-type carbonate preservation pattern at ODP 1240 (Fig. S1) suggests that intensified partial dissolution at only interglacials that may bias IKTF-SSTs toward warmer or bias Mg/Ca-SSTs toward colder. As a result, fluctuations of possible faunal and Mg/Ca-SSTs would be imagined to have been much smaller and greater than our results, respectively. Another approaches of alkenone-derived SSTs indeed are more robust on a severe carbonate dissolution effect. Yet, size fractions of coccolithophorids are easier to laterally transport/redistribute via bottom currents. Thus higher alkenone content and lower SST estimates at Site 1240 could be suspected due to the strong lateral contributions of high-latitude cold waters. However, we found that no positive correlation exists between ODP 1240 alkenone concentration and  $U^{K'}_{37}$ -SST in MIS 15–13 (Fig. 3a and b). This implies that sediment focusing would have a minor impact on our site. Though possible effects mentioned above may cause the observed offsets among proxies, all the estimation yield a smaller magnitude,  $\sim 1$ – $2$  °C glacial cooling in MIS 14 in comparison with other glacials in the late Quaternary (Fig. 3b–d).

#### 4.2. Water mass variability

Factor analysis is performed on our downcore planktic foraminifer compositions (See Supplementary B - 1.1 Micropaleontological Analysis; 1.2. Q-Mode Factor Analysis), revealing that the Equatorial factor has a relatively smooth amplitude at MIS 16–13, whereas three major components, the EBC, Subtropical, and Subpolar factors possess profound oscillations (Fig. 4). In this interval, the EBC factor is negatively correlated with the Subtropical

( $r = -0.83$ ) and Subpolar factors ( $r = -0.62$ ). The EBC factor (*N. pachyderma* (R), *G. bulloides*, and *N. pachyderma* (L) dominated) has the highest loadings at glacial stages, whereas the lowest of the Subtropical (dominant species: *G. ruber*, *G. glutinata*, and *G. sacculifer*) and Subpolar factors (dominant species: *G. bulloides*, *G. infalta*, *N. pachyderma* (L), and *G. truncatulinoides* (R)) are synchronously observed.

Greater EBC loadings and higher abundances of *Neogloboquadrina pachyderma* (R) dominate at glacial stages, the MIS 15/14 and MIS 13/12 transitions, and parts of interglacial MIS 15. The observed high EBC values are also coincident with low faunal SSTs (Fig. 4). These are indicative of enhanced advective of nutrient-rich, colder waters along the Southern America coast, and then this cold equatorward current penetrates into our core location around the Panama Basin. Though an enhancement of PCC components would leave EBC signatures at Site 1240, other candidates with high abundances of *N. pachyderma* (R) species (such as local equatorial upwelling) could still share partial EBC loadings. By contrast, greater subtropical and subpolar components are nearly synchronized at interglacial stages, which occur in conjunction with warmer SST estimates (Fig. 4). This signals a shift from cold PCC-dominated at glacial periods to more subpolar/subtropical waters at interglacials. One possible explanation is that the supply of subtropical and subpolar waters at interglacials could be carried by reinforced/extended South Pacific subtropical gyre circulations, and then indirectly weaken/halt the PCC influx entering our site. This feature is in good agreement with the minimum values of EBC loadings/*N. pachyderma* (R) abundances or even fully absent at interglacials. However, we find more dissolved interglacials (>30% of planktic foraminiferal fragment index; a

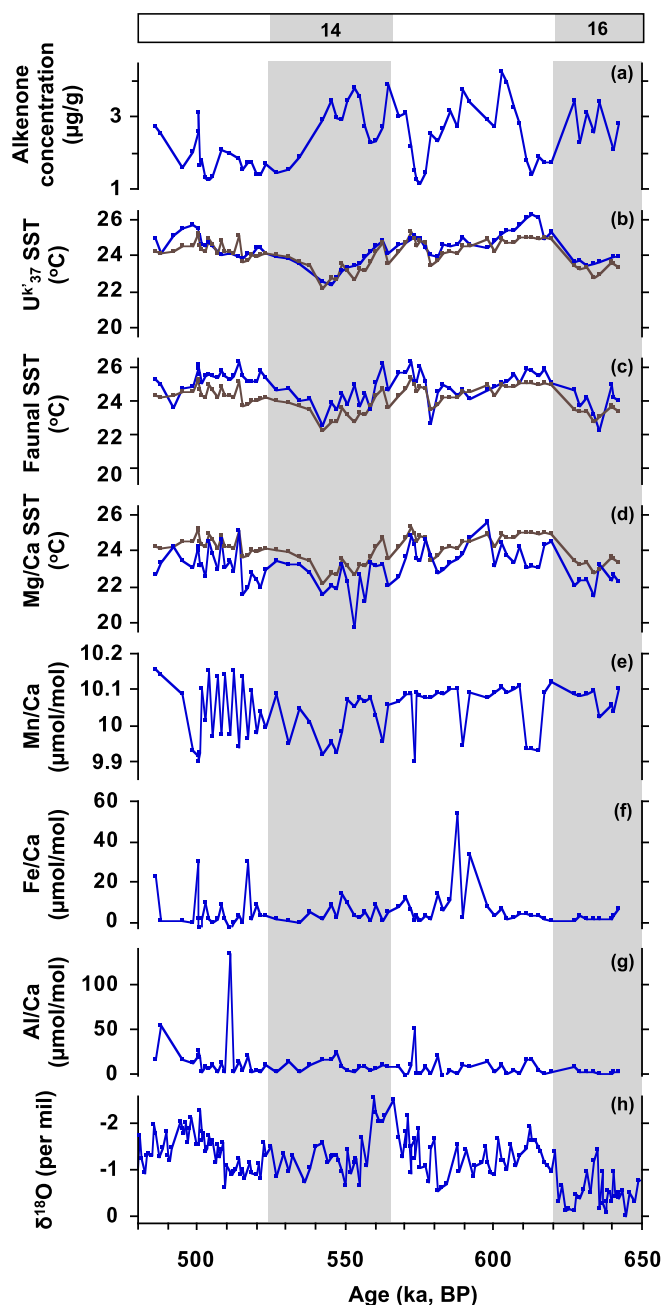


**Fig. 3.** Downcore ODP 1240 SST estimations derived from multiple indices were during MIS 16–13 intervals. (a) Alkenone concentration; (b–d)  $U^{k}_{37}$ -based SST, faunal-based SST from IKTF-type methods and foraminiferal Mg/Ca-SST estimates with multiple mean SST (red line); (e–g) the major trace elements Mn/Ca, Fe/Ca, Al/Ca, all plotted against age and compared to (h) downcore  $\delta^{18}O$  stratigraphy. Shaded intervals indicate glacial periods. (For interpretation of the references to colour in this figure legend, the reader is referred to the web version of this article.)

ratio of fragmented to whole planktic foraminifera; Fig. S1) would cause the near disappearance of small calcite tests of *N. pachyderma* (R) (Fig. 4). We further observe high dissolution-resistant *Globorotalia crassformis* abundances and the lowest communalities (<0.8) extracted from a modified faunal factor matrix (Yu et al., 2012) in a particularly poor carbonate preservation interval of ~590–582 ka (Fig. S1). The existence of no-analogue conditions of very high *Globorotalia crassformis* abundances that could not be found from EEP coretops would bias and lead to under-estimating downcore faunal-SSTs.

## 5. Discussion

### 5.1. Assessment of multiple SST estimates

The higher SSTs of our multi-technique estimates mainly occur at interglacial periods and the lower SSTs occur during glacial stages (see Result 4.1; Fig. 3), but biases and discrepancies among these multiple temperature proxies remain. Our multiple temperature methods result from the species composition of two functional groups: coccolithophorids and planktic foraminifera. Earlier investigations of sediment traps at Hawaii/Bermuda and culture experiments indicate differences in sensitivity to environmental factors such as the depth habitat of mixed layer depths. Light and nutrient availability on coccolithophorids could cause  $U^{k}_{37}$ -SST biases (Cortes et al., 2001; Haidar and Thierstein, 2001; Prahl et al., 2006). At Site 1240 where there is a steeper temperature depth profile and below 20 m water depth, minor seasonal changes are observed (WOA, 1998; Locarnini et al., 2010), indicating a well-mixed water column (i.e. mixed layer and thermocline depth) occupies Site 1240 year-round. Though a preferred annual cold oceanic environment with nitrate-rich would be adaptable for alkenone-related species in coccolithophorids production and *N. dutertrei*-dominating in planktic foraminifera. Previous studies have viewed the  $U^{k}_{37}$ -SST index as a specific seasonal signal (i.e. winter season), which is associated with seasonal blooms of coccolithophorids. An example in the SCS record is inferred to be due to an enhancement of the East Asian winter monsoon (Steinke et al., 2008). Taking the local hydrographic conditions with well-mixed water columns annually in the EEP into account, we think that our alkenone-SSTs reflect more annual mean of hydrographic signal compared to the other two proxies.

In terms of Mg/Ca analysis, little is known about the depth habitats and isotopic/temperature differences of two *G. ruber* morphotypes (s.s./s.l.) at the EEP. Sediment trap experiments at the north Pacific subtropical gyre reveal that the isotopic discrepancy could be attributed to ~1 °C differences in their habitation depths (Kawahata, 2005). Therefore higher ratio of *G. ruber* morphotypes (s.s./s.l.) being employed in Mg/Ca SST measurements would bring more surface, and probably annual mean signals. Reconstructions of the southern SCS temperature records further confirm that a ~1.1 °C difference between the morphotype-specific mean SSTs during the last deglaciation is due to the depth of their habitats (Steinke et al., 2008). Here we speculate that their ecology and vertical distribution in the EEP water column are not sensitive to a regional hydrography such as the SCS. In fact, coretop distribution of *G. ruber* in the Pacific indicates no major changes in surface hydrography and more homogeneous EEP oceanic environments. The resulting temperature differences at *G. ruber* s.s./s.l. would be not that large in the EEP. If this is the case, the bias of our Mg/Ca SST estimation would mainly reflect the ratio of *G. ruber* morphotypes (s.s./s.l.) that have been measured for this study. Due to more *G. ruber* s.l. specimens with relatively deeper habitat have been used in our Mg/Ca SST analysis, our Mg/Ca-SSTs would be representative for colder extreme or winter conditions.

In addition, potential temperature biases may be derived from no-analogue condition and also poor carbonate preservation. For better constraint on these issue, a modified IKTF-type (without *Globorotalia menardii* + *Globorotalia tumida* species) is applied to our downcore fauna samples (Yu et al., 2012). Our faunal IKTF-SST estimates with greater biases at interglacial stages would result from poor carbonate preservation. An extreme case of a no-analogue condition at ~590–582 ka would amplify temperature biases as evidenced by lowest values in communality (Fig. 4). Our faunal SSTs would be also somewhat under-estimated at interglacial stages due to the removal of warm but dissolution-susceptible

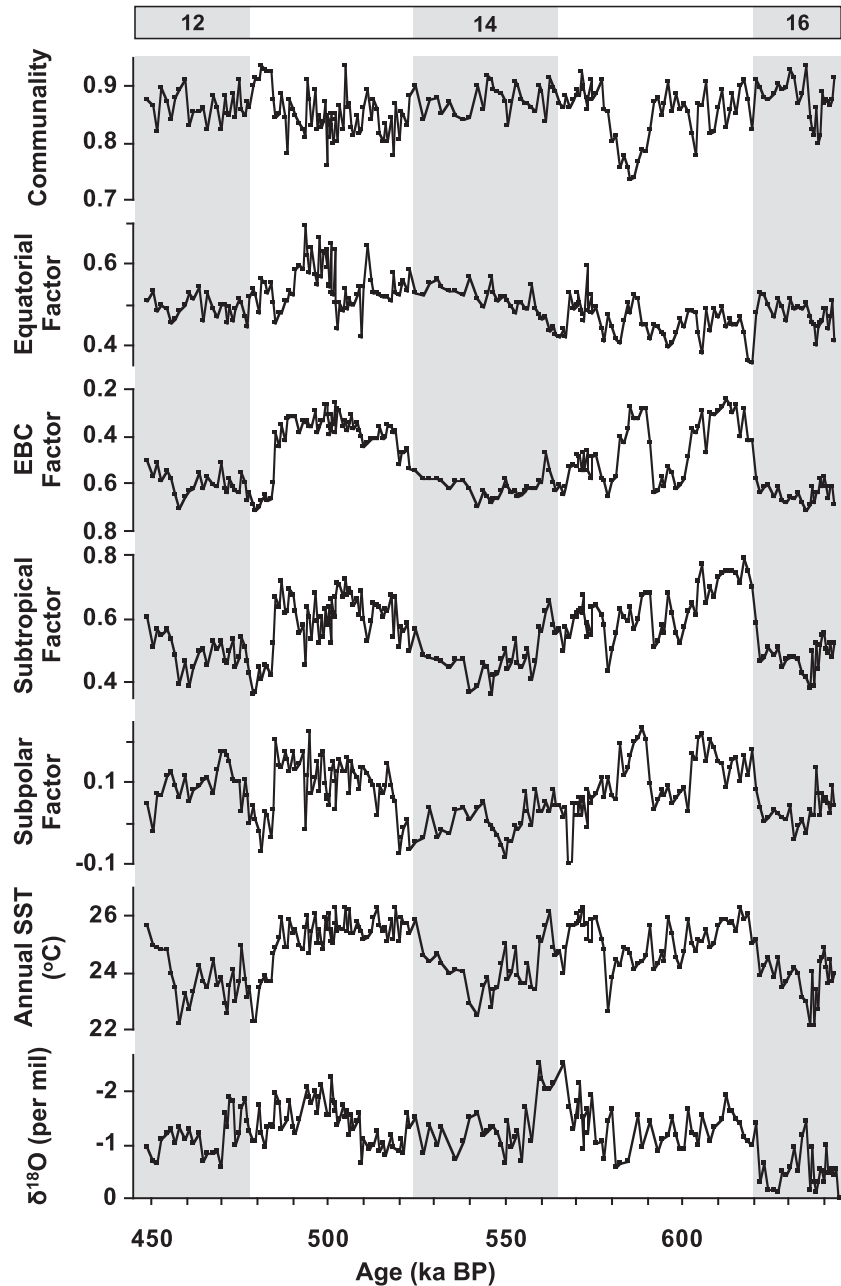


**Fig. 4.** ODP Site 1240 planktic foraminifer fauna factors (i.e., communality, Equatorial, EBC, Subtropical, and Subpolar components) derived from a Q-mode factor analysis of a EP regional calibration data set (Yu et al., 2012), compared to modified IKTF-type estimated annual mean SSTs, and seasonality of the SSTs for MIS 16–13 intervals. All data are plotted against age and compared to downcore  $\delta^{18}\text{O}$  stratigraphy. Shaded intervals indicate glacial periods.

species such as *G. ruber* and *G. sacculifer*. Furthermore, Prahl et al. (2006) suggest that a similar no-analogue condition could exist with EEP alkenone/alkenoate signatures, thereby reflecting the fact that the LGM ecology of phytoplankton producing these biomarkers was different from today. This is in agreement with a similar feature that has been observed in the equatorial and south Atlantic, particularly in upwelling regions associated with an EBC system (Niebler et al., 2003). Though there is insufficient information available to study the non-thermal physiological impacts on both culture experiments and downcore samples, here we suggest that the no-analogue condition could cause minor uncertainties in the fauna-SST estimates.

Other factors such as contamination effects on Mg/Ca analysis

(Lea et al., 2005) and a lateral transport effect on coccolithophorids (Kienast et al., 2006; Dubois et al., 2009) have been mentioned in previous EEP investigations. Around the Galapagos Islands we consider the possibility that foraminifer shells adhered to local volcano materials could be restricted off the northern areas as compared with major trace metal analysis from our results and Pena et al. (2005). Thus a warmer bias would be recorded at Site TR163–19 (Lea et al., 2005), but not Site ODP 1240. On the other hand,  $^{230}\text{Th}$  normalized flux from ME0005A-24JC ( $0^{\circ}1.3'\text{N}$ ,  $86^{\circ}27.8'\text{W}$ ), which is almost same site of ODP 1240, has verified that an increased LGM sedimentation rate could result from a local lateral transport effect, resulting in fine particles being redistributed/winnowed by bottom currents, and even bringing on inaccuracy of

age models (Kienast et al., 2006, 2007). In the case of similar geography, the impact of the first two factors would happen in limited areas to a lesser degree, and thus could have minor effect on  $U^{K}_{37}$ -SST estimates (Kienast et al., 2006; Dubois et al., 2009). In fact, no clear correlation between alkenone concentration and  $U^{K}_{37}$ -SSTs at ODP 1240 or its nearby Site ODP 846/849 (McClymont and Rossel-Mele, 2005; Liu et al., 2008) further suggests a minimal lateral transport effect on our records.

In summary, all these observed discrepancies in our multi-SST estimates could be ascribed to the different sensitivities of the SST methodologies themselves, or different optimum growing seasons of planktic foraminifera and coccolithophorids, and/or a degree of different ratios in selecting of *G. ruber* s.s./l. specimens for Mg/Ca analysis. Our multiple proxies therefore unanimously indicate that, in glacial MIS 14, a reduced cooling ( $\sim 1$ – $2$  °C; Fig. 3) at ODP 1240 is not limited to any specific season, but is a year-round pattern.

## 5.2. EEP climate scenarios in interglacial-like MIS 14

With multiple SSTs of Site 1240, we are able to assess magnitude of EEP cooling and water masses variability in interglacial-like MIS 14 (Figs. 3 and 4). In comparison with published multi-SST records around the EEP, we found that the magnitude of EEP MIS 14 cooling is smaller in comparing to other glacials (Fig. 5; Pisias and Rea, 1988; Chen, 1994; McKenna et al., 1995; Liu et al., 2008). SST records (e.g. ODP 846/1240) from near the center of the cold tongue are also characterized by reduced cooling in MIS 14 (Liu et al., 2008; This study). It could be hypothesized that the contribution of high-latitude cold water weakens, or a flux of cold tongue entering the EEP decreases during MIS 14 (Fig. 6). Benthic foraminifer  $\delta^{13}C$  signatures off the Peru margin indicate that an enhancement of the ACC in MIS 14 would bring high-latitude cold upwelled waters into the EEP (Mohtadi et al., 2006). Faunal results from Site 1240 obtained from the dominant species *N. pachyderma* (R), *G. bulloides* and *N. pachyderma* (L) during MIS 14 suggest a strong EBC system (Fig. S1). Taking the DOT-ventilated process into account (Yu et al., 2012), we postulate that there was a closing of the oceanic tunnel blocking subpolar water masses, or a subtropical gyre expanding into the Panama Basin in MIS 14 (Fig. 4). This interpretation is also consistent with the temporary absence of subpolar fauna *G. inflata* at ODP 1240, suggesting a lack of nutrient-rich, cool environment adapted for fauna production around the Panama Basin. A similar situation has been reported in the Atlantic, in that the abrupt appearance of giant diatom ooze *Ethmodiscus rex* in the southern subtropical Atlantic also suggests a warm subtropical gyre and an equatorward shift of southern westerlies in MIS 14 (Rackebrandt et al., 2011). This suggests that the subtropical warm waters via the Gulf Stream would be transported toward the EEA and had a substantial influence on the thermal structure and hydrography of the Caribbean Sea (Rackebrandt et al., 2011), and the same surface circulation pattern has been developed in the EEP in MIS 14 (Fig. 6).

An atmospheric bridge may also play a role in determining the surface circulation pattern in the EEP (Liu and Yang, 2003). Taking an example for the Atlantic, we consider that the latitudinal position of the ITCZ in MIS 14 would lie between the Caribbean Sea MD03-2628 (Sepulcre et al., 2011) and EEP ODP 846/ODP 847/ODP 1240 (Chen, 1994; McKenna et al., 1995; Liu et al., 2008; This study), as evidenced by these SST variations (Fig. 6). The flux of heat and water vapors around the EEA is easily exchanged across the Isthmus of Panama into the EEP via southward shifts of the ITCZ with its cross-equatorial trade winds. This would induce an expansion of the oligotrophic tropical warm water at the EEP warm pool. In the tropical Andes, more arid climate conditions are also due to an intensification of the southeastern trade winds (Hooghiemstra

et al., 1993). For the glacial MIS 14 scenario of the EEP, we suggest that though the EEP would receive more nutrient-rich, cold waters from high latitudes that in turn would drive more westward extension of the equatorial cold tongues. The atmospheric bridge of a more southward ITCZ position in the EEP blocks more efficiently than the ocean transport and therefore weakens the EEP cold tongue more substantially in MIS 14. Therefore, we suggest that the EEP in glacial MIS 14 is characterized by a reduced development of EEP cold tongue, as evidenced by the SST records of ODP 1240 and ODP 846 (Figs. 5 and 6).

## 5.3. Possible mechanism for glacial MIS 14 EEP climate

### 5.3.1. Orbital variations

A variety of ocean climate records from the low-latitude regions have suggested that the tropical processes played an extremely important role in controlling global climate changes. For better addressing the specific climate patterns in glacial MIS 14, we offered another perspective on how tropical dynamics and high-to-low latitudes interaction have been co-evolved in the EEP, and proposed a reasonable explanation. First, the orbital variations in glacial MIS 14 were characterized by higher obliquity fluctuations, lower eccentricity/precession (Fig. 5). Increase of obliquity would enhance inter-hemispheric asymmetry and therefore amplify the magnitude of seasonality (i.e. colder winters and hotter summers) (Imbrie et al., 1984). If this obliquity oscillation triggered effectively a unique MIS 14 basin-wide event across the tropical oceans, a remote forcing must have accompanied by dynamic oceanic tunnels and/or atmospheric bridges, to allow these extra-tropical climate effects be transmitted to the tropics (e.g. Liu and Yang, 2003). Previous EEP SST archives have demonstrated that both high and low-latitude SST variations seem to respond in phase to obliquity forcing (Liu et al., 2008; Pena et al., 2008). The obliquity component of the SSTs would have a close tele-connection with the climate response of the Southern Ocean, and thus be conveyed by possible pathways of SAMW and/or advection of the PCC (Pisias and Mix, 1997). In this scenario, a globally co-varying cooling phenomena could be generated in either high or low latitude areas during the same interval. However, one argument against this idea is that WPWP marine cores (de Garidel-Thoron et al., 2005; Medina-Elizalde and Lea, 2005), East Asia terrestrial archives (e.g. Sun et al., 2005; Cheng et al., 2016) and even northern Pacific records (Matsuzaki et al., 2014) cannot be fully explained by this extra-tropical forcing. Low-latitude oceans/East Asia terrestrial regimes would still maintain their relatively warm and/or humid states rather than undergoing cooling during upwelling episodes in the EEP (Yu and Chen, 2011) and tropical Atlantic. A model simulation study of the tropical Pacific responding to obliquity forcing has revealed that during a maximum in obliquity, a one-fifth weakening of the subtropical gyre circulation would occur relative to minimum obliquity (Lee and Poulsen, 2005). Therefore, it is possible that the warmth of the south Pacific/Atlantic subtropical gyre and an equatorward shift of southern westerlies in MIS 14 could have been driven by the oceanic mechanism (Mohtadi et al., 2006; Rackebrandt et al., 2011).

### 5.3.2. Greenhouse gas effect

In the light of greenhouse gas effects, atmospheric  $CO_2$  and  $CH_4$  concentrations retrieved from Antarctic ice core records (Louergue et al., 2008; Luthi et al., 2008; Petit et al., 1999) seem to suggest another possible candidate to link multiple records across the different oceanic basins. Over the last 400 kyr, the  $CO_2$  (or  $CH_4$ ) contents varied by  $\sim 180$  ppm ( $\sim 400$  ppb) in glacials, compared to  $\sim 280$ – $300$  ppm ( $\sim 600$ – $700$  ppb) in interglacials (Louergue et al., 2008; Luthi et al., 2008). If greenhouse forcing was the sole factor

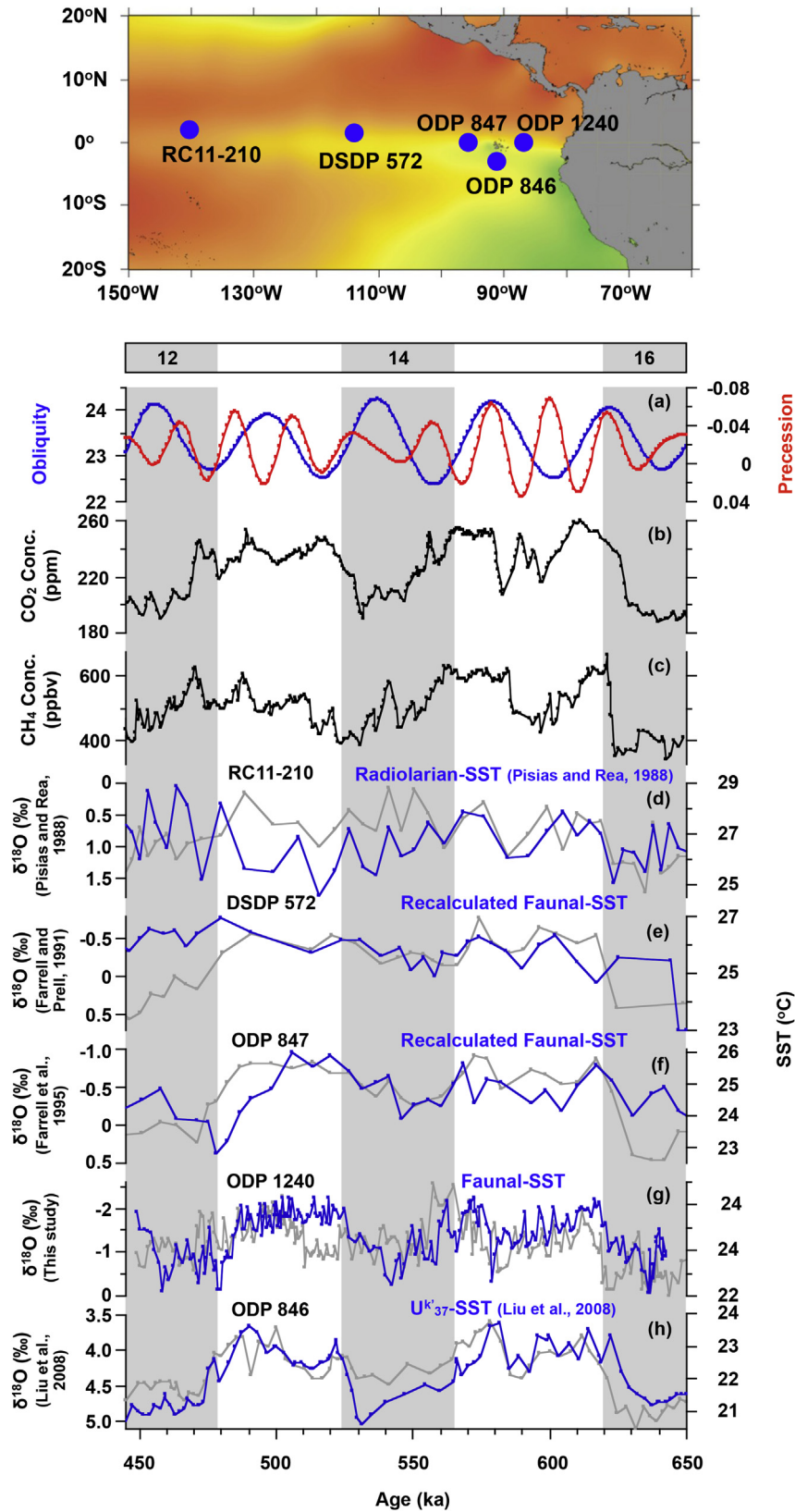


**Fig. 5.** During MIS 16–12 eastern tropical Pacific climate proxy records, orbital-forcing obliquity/precession index, and greenhouse gases contents in EPICA Dome C (EDC) ice core. (a) Obliquity (blue line)/Precession index (red line) (Laskar et al., 2004); (b) atmospheric CO<sub>2</sub> concentration in EDC ice core (Luthi et al., 2008); (c) atmospheric CH<sub>4</sub> concentration in EDC ice core (Louergue et al., 2008); (d) radiolarian-based SSTs and  $\delta^{18}\text{O}$  stratigraphy of core RC11-210 (Pisias and Rea, 1988); (e) IKTF-based SSTs and  $\delta^{18}\text{O}$  stratigraphy of a DSDP core 572 (Farrell and Prell, 1991; Chen, 1994; this study); (f) IKTF-SSTs and  $\delta^{18}\text{O}$  stratigraphy of Core ODP 847 (Chen, unpublished data; Farrell et al., 1995; McKenna et al., 1995; this study); (g) IKTF-SSTs and  $\delta^{18}\text{O}$  stratigraphy of Core ODP 1240 (this study) and (h)  $U^{37}$ -SSTs and  $\delta^{18}\text{O}$  stratigraphy of Core ODP 846 (Liu et al., 2008).  $\delta^{18}\text{O}$  stratigraphy showed in grey and SST showed in blue. Shaded intervals indicate glacial MISs. (For interpretation of the references to colour in this figure legend, the reader is referred to the web version of this article.)

## Glacial MIS 14 Scenario

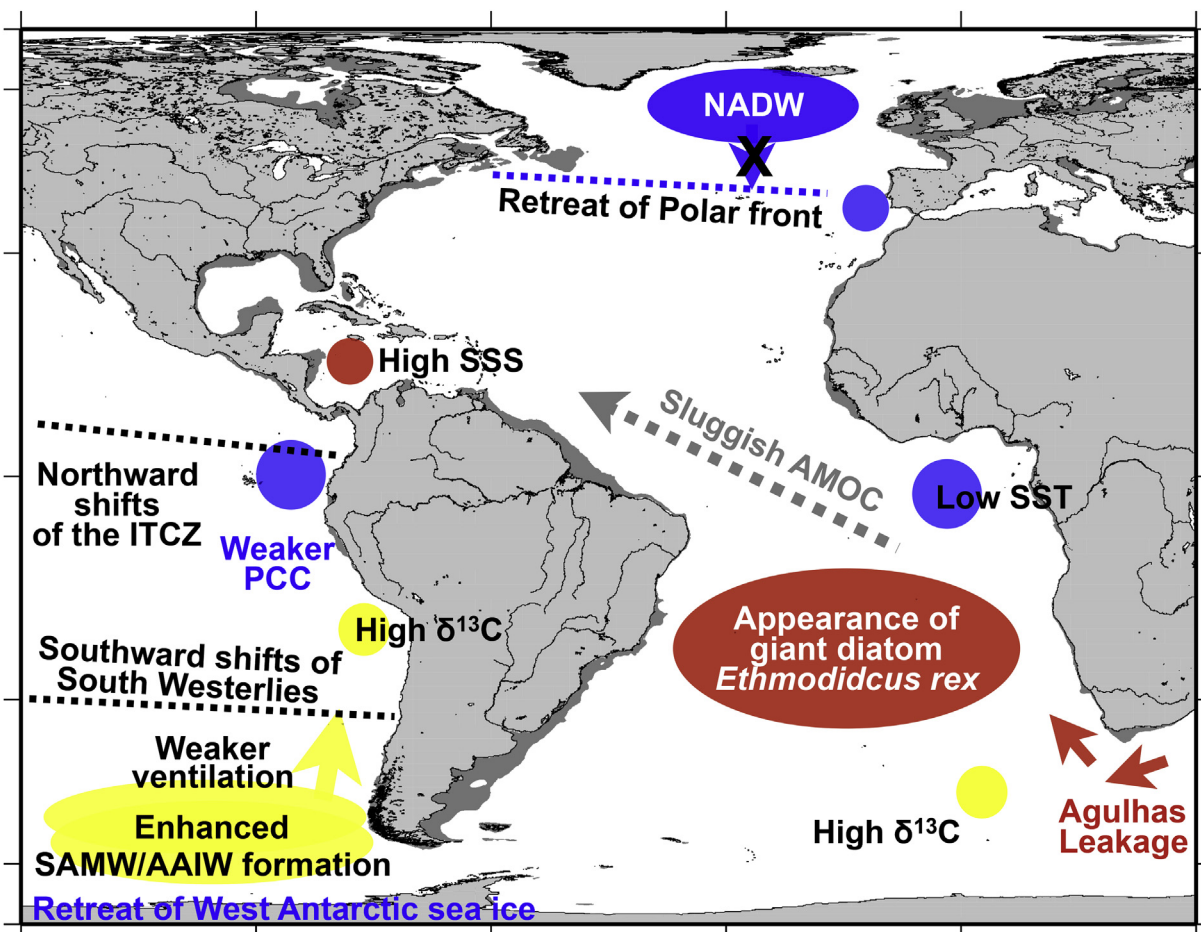


Fig. 6. Schematic diagrams illustrating the inferred paleoclimatic conditions of the EP in glacial 14 based on data reviewed in this study.

responsible for modifying global climate at orbital time scales, a double emission of  $p\text{CO}_2$  content would cause a 4.4–5.6 °C warming in eastern tropical upwelling zones, a suggestion that tropical climate sensitivity would have been driven totally by  $p\text{CO}_2$  variation (Lea, 2004). Thus, a synchronously cooling feature in MIS 15–13 would be ubiquitously observed, and a similar SST variation (–2–3 °C; 70 ppm in  $p\text{CO}_2$ ) also would be recorded in the tropical areas (Fig. 5). However, a variety of SST records from the low-latitude Pacific reveal inconsistent responses in terms of this greenhouse gas effect. While faunal-derived SST estimates in EEP (Site 1240) exhibited a maximum cooling (–4 °C; Fig. 5), evidence from the stability of WPWP instead indicates minimal or no change in SST (de Garidel-Thoron et al., 2005; Medina-Elizalde and Lea, 2005; Shiau et al., 2008; Yu and Chen, 2011). This significant east-west SST gradient along the cross-equatorial Pacific clearly conflicts with a possible global cooling pattern driven by the greenhouse forcing. More importantly, changes in  $p\text{CO}_2$  content, as well as an obliquity forcing response, was a tropical trigger of the MIS 14 cooling in both high and low latitudes. Thus this greenhouse effect alone would not fully drive tropical climate changes, but it may interact with other climate mechanisms (e.g. obliquity forcing) or be one of several important non-linear components. This active and highly non-linear role in global climate change would lead to inconsistent evidence from glacial MIS 14.

### 5.3.3. Atmospheric and oceanic interactions

For the paradox of interglacial-like glacial MIS 14 climate, we also considered other possibly involved climate mechanisms, interactions and/or feedbacks to drive such interglacial-like MIS 14 climate. The rate and variability of SAMW formation had a direct effect on Atlantic Meridional Ocean Circulation (AMOC) behavior via oceanic tunnels. Thus, the changes of AMOC pattern would be another key component for setting up the meridional asymmetry in the Atlantic and Pacific climate in MIS 14 (Duplessy et al., 1988; Sarnthein et al., 1994). The benthic foraminifera  $\delta^{13}\text{C}$  as a tracer of deep water circulation has been measured from highly location-dependent marine cores that were retrieved at adequate water depths, close to the path of the AMOC circulations (Boyle and Keigwin, 1982; Oppo and Lehman, 1993; Vidal et al., 1998). Though the precise extent and pattern of AMOC during the late Quaternary are still unknown, a depletion of the MIS 14  $\delta^{13}\text{C}$  record from the tropical Atlantic Ocean (Raymo et al., 1997; Ruddiman et al., 1989) suggests a weaker or even an inactive AMOC. This is supported by what has been recorded in Iberian Margin alkenone SST records, suggesting the advection of subtropical water masses entering this area was due to the retreat of the polar front (MD03-2699 in Rodrigues et al., 2011).

However, it could be argued that regional distributions of limited benthic  $\delta^{13}\text{C}$  records are insufficient for describing MIS 14

thermohaline circulation variations because overturning signals mainly depend upon specific site locations. Benthic foraminifera  $\delta^{13}\text{C}$  records of the eastern Pacific (Raymo et al., 1997, 2004; Mohtadi et al., 2006) suggest that a tele-connection of North Atlantic ventilated water would shut down or be stagnant during this interval. This is also supported by planktic foraminiferal fragment index of our EEP Site 1240 that documented a synchronously weakening foraminiferal dissolution event in MIS 14 (Fig. S1). Thus, this shrunken or weakened global conveyor belt in MIS 14 would redistribute the heat in the ocean on a global scale, and further increase the inter-hemispheric contrast. Analyses of coupled climatic models provide a plausible connection between the thermohaline circulation and remote regions of the tropics (Fig. 6). A freshwater forcing occurring in the northern Atlantic would induce a poorly ventilated or stagnant ventilated deep water, and then a southward shift of ITCZ in the tropical Atlantic and the EEP (Zhang and Delworth, 2005; Vellinga and Wood, 2002). Thus, more flux of heat and moisture could be transported into the EEP (Fig. 6). As a consequence, we speculate that the EEP upwellings in glacial MIS 14 would be accomplished with slightly colder SST and highly saline conditions, as estimated from planktic foraminifer  $\delta^{18}\text{O}$  and SST signatures (Fig. 5). Therefore, a possible more La Niña-like phase in glacial MIS 14 resulting from the interaction between tropical and extra-tropical mechanisms may have linked the ITCZ/EBC systems and heat/water vapor transport, which in turn, serve a more plausible explanation for the interglacial-like climate in MIS 14.

In summary, we suggest that multiple climatic mechanisms, including the obliquity forcing, atmospheric  $\text{CO}_2$  effects, remote forcing from high latitude processes, and the ITCZ shift/oceanic circulation pattern changes, all need to be considered to better explain these zonal meridional temperature gradients of the EEP upwellings during MIS 14. In order to fully understand the global expression of the tropical dynamics, future research should not only assemble enough terrestrial/marine records from subtropical areas, the western equatorial Atlantic Ocean, and the WPWP, but also gather sufficient information on variations in climate/oceanic fronts, the behavior of warm pools and long-term La Niña-like climate patterns, and possible linkages between ITCZ migration and monsoon systems. In experiments with idealized coupled climate models for glacial MIS 14, further modeling investigations will be needed to confirm the air-sea interaction, its linkage between the oceans, and interactions with other boundary conditions (i.e., atmospheric  $\text{CO}_2$  content, orbital forcing, solar insolation, etc.) in interglacial-like MIS 14.

## 6. Conclusions

In this study, we have documented surface hydrographic and water mass variations of the EEP Site ODP 1240 spanning MIS 15–13 as revealed by multiple SSTs and planktic foraminifer compositions. Based on our analysis with particular focus on an interglacial-like MIS 14 interval, our study provided four main insights related to the regional and global linkage of atmospheric/oceanic processes:

- 1 In this study, multiple temperature estimates of ODP 1240 based on the EP IKTF, alkenone index  $U^{K}_{37}$ , and Mg/Ca ratios on *G. ruber* s.s./s.l. successfully demonstrate significant EEP cooling and water masses variability during the MIS 16–13 interval. ODP 1240 multiple SSTs show  $\sim 1\text{--}2\text{ }^\circ\text{C}$  glacial cooling in MIS 14 in comparison with other glacials in the late Quaternary;
- 2 In comparison with published multi-SST records around the EEP, we found that the magnitude of EEP MIS 14 cooling is smaller in comparing to other glacials. SST records (e.g. ODP 1240/846) from near the center of the cold tongue are also characterized by

reduced cooling in MIS 14. The strong cooling ( $\sim 4\text{ }^\circ\text{C}$ ) shown in our ODP 1240 faunal-based record corresponds to an increase in the EBC factor, suggesting that the PCC water mass contributed to cooling in the EEP;

- 3 Regarding the glacial MIS 14 scenario of the EEP, we further hypothesized that the EEP areas would receive more nutrient-rich, cold waters from high latitudes and also be affected by equatorial cold tongues, as revealed by faunal-derived evidence. However, the atmospheric bridge of a northwardly ITCZ shift and the resulting heat/water vapor transport across the EEA to EEP would reduce effectively the magnitude of cooling in EEP cold tongue in MIS 14;
- 4 When we consider all possible climate mechanisms that could be involved in explaining the paradox of interglacial-like MIS 14, effects exerted from changes in orbital forcing, insolation, and greenhouse gas concentrations cannot solely explain the SST changes and EEP cold tongue variability in glacial MIS 14. For modifying the thermal asymmetry of the climate/oceanic variations in interglacial-like MIS 14, we suggest that future studies should focus on the role of tropical ocean-atmosphere interactions (e.g. ENSO conditions) and/or changes in the AMOC pattern.

## Acknowledgements

This study was supported by the National Taiwan Ocean University and grants (NSC96-2611-M-019-008 & NSC96-2611-M-019-009) to MTC, and by the Graduate Students Study Abroad Program (NSC-096-2917-I-019-101) and grants (NSC102-2116-M-492-002 & MOST 103-2116-M-492-001) to PSY from the National Science Council (NSC)/Ministry of Science and Technology (MOST), Taiwan. MK acknowledges funding from NSERC Canada and CIFAR. The authors would like to thank the crew on the JOIDES *Resolution* during ODP Leg 202 for their drilling and curatorial assistance. We also thank the members who work in the Marine Core Repository and Laboratory at the Taiwan Ocean Research Institute (TORI), National Applied Research Laboratories (NARLabs) for helping us finish the sample processing for this study.

## Abbreviations

AAIW, Antarctic Intermediate Water; ACC, Antarctic Circumpolar Current; EBC, eastern boundary current; EEA, eastern equatorial Atlantic; EEP, eastern equatorial Pacific; EUC, equatorial undercurrent; ETP, orbital forcing includes Eccentricity, Obliquity, and Precession; IKTF, Imbire-Kipp transfer function; MIS, Marine Isotope Stage; MBT, Mid-Brunhes Transition; MPT, mid-Pleistocene climate transition; PCC, Peru-Chile Current; SST, sea surface temperature; SAMW, subantarctic Mode Water; WPWP, western Pacific warm pool.

## Appendix A. Supplementary data

Supplementary data related to this article can be found at <http://dx.doi.org/10.1016/j.quaint.2016.12.021>.

## References

- Altabet, M.A., Murray, D.W., Prell, W.L., 1999. Climatically linked oscillations in Arabian Sea denitrification over the past 1 m.y.: implications for the marine N cycle. *Paleoceanography* 14 (6), 732–743.
- Anand, P., Elderfield, H., Conte, M.H., 2002. Calibration of Mg/Ca thermometry in planktonic foraminifera from a sediment trap time series. *Paleoceanography* 18 (2), 1050. <http://dx.doi.org/10.1029/2002PA000846>.
- Barker, S., Greaves, M., Elderfield, H., 2003. A study of cleaning procedures used for foraminiferal Mg/Ca paleothermometry. *Geochim. Geophys. Geosystems* 4 (9), 8407. <http://dx.doi.org/10.1029/2003GC000559>.

- Bassinot, F.C., Labeyrie, L., Vincent, E., Quidelleur, X., Shackleton, N.J., Lancelot, Y., 1994. The astronomical theory of climate and the age of the Brunhes-Matuyama magnetic reversal. *Earth Planet. Sci. Lett.* 126 (1–3), 91–108. [http://dx.doi.org/10.1016/0012-821X\(94\)90244-5](http://dx.doi.org/10.1016/0012-821X(94)90244-5).
- Berger, W.H., Bickert, T., Jansen, E., Wefer, G., Yashuda, M., 1993. The central mystery of the Quaternary ice age: a view from the South Pacific. *Oceanus* 36, 53–56.
- Boyle, E.A., Keigwin, L.D., 1982. Deep circulation of the North Atlantic over the last 200,000 years: geochemical evidence. *Science* 218, 784–787.
- Chen, M.-T., 1994. Late Quaternary Paleoceanography of the Equatorial Indo-Pacific Ocean: a Quantitative Analysis Based on Marine Micropaleontological Data. Ph.D. thesis. Brown University.
- Cheng, H., Edwards, R.L., Sinha, A., et al., 2016. The Asian monsoon over the past 640,000 years and ice age terminations. *Nature* 534 (7609), 640–646. <http://dx.doi.org/10.1038/nature18591>.
- Clemens, S.C., Murray, D.W., Prell, W.L., 1996. Non-stationary phase of the Pliocene-Asian monsoon. *Science* 274, 943–948.
- Clemens, S.C., Prell, W.L., Sun, Y., Liu, Z., Chen, G., 2008. Southern Hemisphere forcing of Pliocene  $\delta^{18}\text{O}$  and the evolution of Indo-Asian monsoons. *Paleoceanography* 23, PA4210. <http://dx.doi.org/10.1029/2008PA001638>.
- Cortés, M.Y., Bollmann, J., Thierstein, H.R., 2001. Coccolithophore ecology at the HOT station ALOHA, Hawaii. *Deep Sea Res. Part II* 48, 1957–1981.
- de Garidel-Thoron, T., Rosenthal, Y., Bassinot, F., Beaufort, L., 2005. Stable sea surface temperatures in the western Pacific warm pool over the past 1.75 million years. *Nature* 433, 294–298.
- Droxler, A.W., Alley, R.B., Howard, W.R., Poore, R.Z., Burckle, L.H., 2003. Unique and Exceptionally Long Interglacial Marine Isotope Stage 11: Window into Earth Warm Future Climate, vol. 137. American Geophysical Union, Washington D.C. <http://dx.doi.org/10.1029/137GM01>, 5–4.
- Dubois, N., Kienast, M., Normandeau, C., Herbert, T.D., 2009. East equatorial Pacific cold tongue during the Last Glacial Maximum as seen from alkenone paleothermometry. *Paleoceanography* 24, PA4207. <http://dx.doi.org/10.1029/2009PA001781>.
- Duplessy, J.C., Shackleton, N.J., Fairbanks, R.G., Labeyrie, L.D., Oppo, D., Kallel, N., 1988. Deepwater source variations during the last climatic cycle and their impact on the global deepwater circulation. *Paleoceanography* 3 (3), 343–360.
- Farrell, J.W., Prell, W.L., 1991. Pacific  $\text{CaCO}_3$  preservation and  $\delta^{18}\text{O}$  since 4 Ma: Paleocenic and paleoclimatic implications. *Paleoceanography* 6, 485–498.
- Farrell, J.W., Murray, D.W., McKenna, V.S., Ravelo, A.C., 1995. Upper ocean temperature and nutrient contrasts inferred from Pleistocene planktonic foraminifer  $\delta^{18}\text{O}$  and  $\delta^{13}\text{C}$  in the eastern equatorial Pacific. In: Pisias, N.G., Mayer, L.A., Janecek, T.R., Palmer-Julson, A., van Andel, T.H. (Eds.), Proceedings of the Ocean Drilling Program, Scientific Results, vol. 138. Ocean Drilling Program, College Station, Texas, USA, pp. 289–319.
- Flores, J.-A., Wei, W., López-Otálvaro, G.E., Alvarez, C., Sierro, F.J., 2006. Data report: tropical and equatorial calcareous nannofossil Pleistocene biostratigraphy, ODP Leg 202. In: Tiedemann, R., Mix, A.C., Richter, C., Ruddiman, W.F. (Eds.), Proceedings of the Ocean Drilling Program - Scientific Results, vol. 202. Ocean Drilling Program, College Station, Texas, USA, pp. 1–10.
- Haidar, A.T., Thierstein, H.R., 2001. Coccolithophore dynamics off Bermuda (N. Atlantic). *Deep Sea Res. Part II* 48, 1925–1956.
- Heslop, D., Dekkers, M.J., Langereis, C.G., 2000. Timing and structure of the mid-Pleistocene transition: records from the loess deposits of northern China. *Palaeogeogr. Palaeoclimatol. Palaeoecol.* 185, 133–143.
- Hooghiemstra, H., Melice, J.L., Berger, A., Shackleton, N.J., 1993. Frequency spectra and paleoclimatic variability of the high-resolution 30–1450 ka Funza I pollen records (Eastern Cordillera, Colombia). *Quat. Sci. Rev.* 12, 141–156.
- Howell, P., 2001. ARAND Time Series and Spectral Analysis Package for the Macintosh. Brown University.
- Imbrie, J., Hays, J.D., Martinson, D.G., McIntyre, A., Mix, A.C., Morley, J.J., Pisias, N.G., Prell, W.L., Shackleton, N.J., 1984. The orbital theory of Pleistocene climate: support from a revised chronology of the marine  $\delta^{18}\text{O}$  record. In: Berger, A., Imbrie, J., Hays, J.D., Kukla, G., Saltzman, B. (Eds.), Milankovitch and Climate, Part 1. Reidel, Dordrecht, pp. 269–305.
- Kawahata, H., 2005. Stable isotopic composition of two morphotypes of *Globigerinoides ruber* (white) in the subtropical gyre in the North Pacific. *Paleontol. Res.* 9, 27–35.
- Kessler, W.S., 2006. The circulation of the eastern tropical Pacific: a review. *Prog. Oceanogr.* 69 (2–4), 181–217.
- Kienast, M., Kienast, S.S., Calvert, S.E., Eglinton, T.I., Mollenhauer, G., François, R., Mix, A.C., 2006. Eastern Pacific cooling and Atlantic overturning circulation during the last deglaciation. *Nature* 443 (7113), 846–849.
- Kienast, S.S., Kienast, M., Mix, A.C., Calvert, S.E., François, R., 2007. Thorium-230 normalized particle flux and sediment focusing in the Panama Basin region during the last 30,000 years. *Paleoceanography* 22, PA2213. <http://dx.doi.org/10.1029/2006PA001357>.
- Laskar, J., Robutel, P., Joutel, F., Gastineau, M., Correia, A.C.M., Levrard, B., 2004. A long term numerical solution for the insolation quantities of the Earth. *Astron. Astrophys.* 428, 261–285.
- Lea, D.W., 2004. The 100,000 year cycle in tropical SST, greenhouse forcing, and climate sensitivity. *J. Clim.* 17, 2170–2179.
- Lea, D.W., Pak, D.K., Paradis, G., 2005. Influence of volcanic shards on foraminiferal Mg/Ca in a core from the Galápagos Region. *Geochim. Geophys. Geosystems* 6 (11), Q11P04. <http://dx.doi.org/10.1029/2005GC000970>.
- Lee, S.Y., Poulsen, C.J., 2005. Tropical Pacific climate response to obliquity forcing in the Pleistocene. *Paleoceanography* 20, PA4010. <http://dx.doi.org/10.1029/2005PA001161>.
- Lisiecki, L.E., Raymo, M.E., 2005. A Pliocene-Pleistocene stack of 57 globally distributed benthic  $\delta^{18}\text{O}$  records. *Paleoceanography* 20, PA1003. <http://dx.doi.org/10.1029/2004PA001071>.
- Liu, Z., Cleaveland, L.C., Herbert, T.D., 2008. Early onset and origin of 100-kyr cycles in Pleistocene tropical SST records. *Earth Planet. Sci. Lett.* 265, 703–715.
- Liu, Z., Yang, H., 2003. Extratropical control of tropical climate, the atmospheric bridge and oceanic tunnel. *Geophys. Res. Lett.* 30, 1230. <http://dx.doi.org/10.1029/2002GL016492>.
- Locarnini, R.A., Mishonov, A.V., Antonov, J.I., et al., 2010. World ocean Atlas. 2009. In: Levitus, S. (Ed.), Temperature, vol. 1. NOAA Atlas NESDIS 68, US Government Printing Office, Washington, DC, pp. 1–184.
- Loulergue, L., Schilt, A., Spahni, R., Masson-Delmotte, V., Blunier, T., Lemieux, B., Barnola, J.-M., Raynaud, D., Stocker, T.F., Chappellaz, J., 2008. Orbital and millennial-scale features of atmospheric  $\text{CH}_4$  over the past 800,000 years. *Nature* 453, 383–386.
- Luthi, D., Floch, M.L., Bereiter, B., Blunier, T., Barnola, J.-M., Siegenthaler, U., Raynaud, D., Jouzel, J., Fischer, H., Kawamura, K., Stocker, T.F., 2008. High-resolution carbon dioxide concentration record 650,000–800,000 years before present. *Nature* 453, 379–382.
- MARGO Project Members, 2009. Constraints on the magnitude and patterns of ocean cooling at the Last Glacial Maximum. *Nat. Geosci.* 2, 127–132.
- Matsuzaki, K.M., Nishi, H., Suzuki, N., Cortese, G., Eynaud, F., Takashima, R., Kawate, Y., Sakai, T., 2014. Paleoceanographic history of the Northwest Pacific Ocean over the past 740kyr, discerned from radiolarian fauna. *Palaeogeogr. Palaeoclimatol. Palaeoecol.* 396, 26–40. <http://dx.doi.org/10.1016/j.palaeo.2013.12.036>.
- McClymont, E.L., Rossell-Mele, A., 2005. Links between the onset of modern Walker circulation and the mid-Pleistocene climate transition. *Geology* 33, 389–392.
- McKenna, V.S., Farrell, J.W., Murray, D.W., Clemens, S.C., 1995. The foraminifer record at Site 847: Paleoceanographic response to late Pleistocene climate variability. In: Pisias, N.G., Mayer, L.A., Janecek, T.R., et al. (Eds.), Proceedings of the Ocean Drilling Program - Scientific Results, vol. 138, pp. 695–714. <http://dx.doi.org/10.2973/odp.proc.sr.138.141.1995>.
- Medina-Elizalde, M., Lea, D.W., 2005. The mid-Pleistocene transition in the tropical Pacific. *Science* 310, 1009–1012.
- Mix, A.C., Tiedemann, R., Blum, P., 2003. Shipboard scientific Party. In: Proceeding of Ocean Drilling Program - Initial Report, vol. 202. <http://dx.doi.org/10.2973/odp.proc.ir.202.2003>.
- Mohtadi, M., Hebbeln, D., Nuñez-Ricardo, S., Lange, C.B., 2006. El Niño-like pattern in the Pacific during marine isotope stages (MIS) 13 and 11? *Paleoceanography* 21, PA1015. <http://dx.doi.org/10.1029/2005PA001190>.
- Mudelsee, M., Schulz, M., 1997. The Mid-Pleistocene climate transition: onset of 100 ka cycle lags ice volume build-up by 280 ka. *Earth Planet. Sci. Lett.* 151, 117–123.
- Niebler, H.-S., Arz, H.W., Donner, B., Multiza, S., Pätzold, J., Wefer, G., 2003. Sea surface temperatures in the equatorial and South Atlantic Ocean during the last glacial maximum (23–19 ka). *Paleoceanography* 18 (3), 1069. <http://dx.doi.org/10.1029/2003PA000902>.
- Oppo, D.W., Lehman, S.J., 1993. Mid-depth circulation of the subpolar North Atlantic during the last glacial maximum. *Science* 259, 1148–1152.
- Pena, L.D., Calvo, E., Cacho, I., Eggins, S., Pelejer, C., 2005. Identification and removal of Mn–Mg-rich contaminant phases on foraminiferal tests: implications for Mg/Ca past temperature reconstructions. *Geochim. Geophys. Geosystems* 6. <http://dx.doi.org/10.1029/2005GC000930>.
- Pena, L.D., Cacho, I., Ferretti, P., Hall, M.A., 2008. ENSO-like variability during glacial terminations and interlatitudinal tele-connections. *Paleoceanography* 23, PA3101. <http://dx.doi.org/10.1029/2008PA001620>.
- Pennington, J.T., Mahoney, K.L., Kuwahara, V.S., Kolber, D.D., Calienes, R., Chavez, F.P., 2006. Primary production in the eastern tropical Pacific: a review. *Prog. Oceanogr.* 69 (2–4), 285–317.
- Petit, J., Jouzel, J., Raynaud, D., Barkov, N., Barnola, J.-M., et al., 1999. Climate and atmospheric history of the past 420,000 years from the Vostok ice core, Antarctica. *Nature* 399, 429–436.
- Pisias, N.G., Mix, A.C., 1997. Spatial and temporal oceanographic variability of the eastern equatorial Pacific during the late Pleistocene: evidence from radiolaria microfossils. *Paleoceanography* 12 (3), 381–393.
- Pisias, N.G., Rea, D.K., 1988. Late Pleistocene paleoclimatology of the central equatorial Pacific: sea surface response to the southeast trade winds. *Paleoceanography* 3 (1), 21–37. <http://dx.doi.org/10.1029/PA003i001p00021>.
- Prahl, F.G., Mix, A.C., Sparrow, M.A., 2006. Alkenone paleothermometry: lessons from marine sediment records off western South America. *Geochim. Cosmochim. Acta* 70, 101–117.
- Prokopenko, A.A., Hinnov, L.A., Williams, D.F., Kuzmin, M., 2006. Orbital forcing of continental climate during the Pleistocene: a complete astronomically tuned climatic record from Lake Baikal, SE Siberia. *Quat. Sci. Rev.* 25, 3431–3457.
- Rackebandt, N., Kuhnert, H., Groeneveld, J., Bickert, T., 2011. Persisting maximum *Agulhas* leakage during MIS 14 indicated by massive *Ethmodiscus* oozes in the subtropical South Atlantic. *Paleoceanography* 26, PA320. <http://dx.doi.org/10.1029/2010PA001990>.
- Raymo, M.E., Oppo, D.W., Curry, W., 1997. The mid-Pleistocene climate transition: a deep sea carbon isotopic perspective. *Paleoceanography* 12, 546–559.
- Raymo, M.E., Oppo, D.W., Flower, B.P., Hodell, D.A., McManus, J.F., Venz, K.A., Kleiven, K.F., McIntyre, K., 2004. Stability of North Atlantic water masses in face of pronounced climate variability during the Pleistocene. *Paleoceanography* 19, PA2008. <http://dx.doi.org/10.1029/2003PA000921>.

- Rodrigues, T., Voelker, A.H.L., Grimalt, J.O., Abrantes, F.F., Naughton, F., 2011. Iberian Margin Sea Surface Temperature during MIS 15 to 9 (580–300 ka): glacial suborbital variability versus interglacial stability. *Paleoceanography* 26, PA1204. <http://dx.doi.org/10.1029/2010PA001927>.
- Rosignol-Strick, M., Paterne, M., 1999. A synthetic pollen record of the eastern Mediterranean sapropels of the last 1 Ma: implications for the time-scale and formation of sapropels. *Mar. Geol.* 153, 221–237.
- Ruddiman, W.F., 2006. Orbital changes and climate. *Quat. Sci. Rev.* 25, 3092–3112.
- Ruddiman, W.F., Raymo, M.E., Martinson, D.G., Clement, B.M., Backman, J., 1989. Pleistocene evolution: northern Hemisphere ice sheets and north Atlantic Ocean. *Paleoceanography* 4 (4), 353–412.
- Sarnthein, M., Winn, K., Jung, S.J.A., Duplessy, J.C., Labeyrie, L.D., Erlenkeuser, H., Ganssen, G., 1994. Changes in East Atlantic deep water circulation over the last 30,000 years: eight time slice reconstructions. *Paleoceanography* 9, 209–267.
- Sepulcre, S., Vidal, L., Tachikawa, K., Rostek, F., Bard, E., 2011. Sea-surface salinity variations in the northern caribbean sea across the mid-Pleistocene transition. *Clim. Past* 7, 75–90. <http://dx.doi.org/10.5194/cp-7-75-2011>.
- Shackleton, N.J., Berger, A., Peltier, W.R., 1990. An alternative astronomical calibration of the lower Pleistocene timescale based on ODP Site 677. *Trans. R. Soc. Edinb. Earth Sci.* 81, 251–261.
- Shackleton, N.J., 2000. The 100,000-year ice-age cycle identified and found to lag temperature, carbon dioxide, and orbital eccentricity. *Science* 289, 1897–1902.
- Shiau, L.J., Yu, P.S., Wei, K.Y., Yamamoto, M., Lee, T.Q., Yu, E.F., Fang, T.H., Chen, M.T., 2008. Sea surface temperature, productivity, and terrestrial flux variations of the southeastern South China Sea over the past 800,000 years (IMAGES MD972142). *Terr. Atmos. Ocean. Sci.* 19, 363–376. [http://dx.doi.org/10.3319/TAO.2008.19.4.363\(IMAGES\)](http://dx.doi.org/10.3319/TAO.2008.19.4.363(IMAGES)).
- Steinke, S., Kienast, M., Groeneveld, J., Lin, L.-C., Chen, M.-T., Rendle-Bühning, R., 2008. Proxy dependence of the temporal pattern of deglacial warming in the tropical South China Sea: toward resolving seasonality. *Quat. Sci. Rev.* 27, 688–700.
- Sun, Y., Clemens, S.C., An, Z., Yu, Z., 2005. Astronomical timescale and palaeoclimatic implication of stacked 3.6-Myr monsoon records from the Chinese Loess Plateau. *Quat. Sci. Rev.* <http://dx.doi.org/10.1016/j.quascirev.2005.07.005>.
- Tian, J., Wang, P., Cheng, X., Li, Q., 2002. Astronomically tuned Plio-Pleistocene benthic  $\delta^{18}\text{O}$  record from South-China sea and Atlantic-Pacific comparison. *Earth Planet. Sci. Lett.* 203 (3–4), 1015–1029. [http://dx.doi.org/10.1016/S0012-821X\(02\)00923-8](http://dx.doi.org/10.1016/S0012-821X(02)00923-8).
- Tiedemann, R., Sarnthein, M., Shackleton, N.J., 1994. Astronomic timescale for the Pliocene Atlantic  $\delta^{18}\text{O}$  and dust flux records of ocean drilling Program site 659. *Paleoceanography* 9, 619–638.
- Toggweiler, J., Dixon, D., Broecker, W., 1991. The Peru upwelling and the ventilation of the South Pacific thermocline. *J. Geophys. Res.* 96, 20467–20497.
- Vellinga, M., Wood, R.A., 2002. Global climate impact of a collapse of the Atlantic thermohaline circulation. *Clim. Change* 54, 251–267.
- Vidal, L., Labeyrie, L., van Weering, T.C.E., 1998. Benthic  $\delta^{18}\text{O}$  records in the North Atlantic over the last glacial period (60–10 kyr): evidence for brine formation. *Paleoceanography* 13, 245–251.
- WOA, 1998. World Ocean Atlas, Version 2. Technical report. National Oceanographic Data Center. Silver Spring, Maryland. <http://www.nodc.noaa.gov/oc5/woa98.html>.
- Yu, P.S., Chen, M.T., 2011. A prolonged warm and humid interval during Marine Isotope Stage 13–15 as revealed by hydrographic reconstructions from the South China Sea (IMAGES MD972142). *J. Asian Earth Sci.* <http://dx.doi.org/10.1016/j.jseaes.2010.08.002>.
- Yu, P.S., Kienast, M., Chen, M.T., Cacho, I., Flores, J.-A., Mohtadi, M., Mix, A.C., 2012. Influences of extratropical water masses on equatorial Pacific cold tongue variability during the past 160 ka as revealed by faunal evidence of planktic foraminifers. *J. Quat. Sci.* 27 (9), 921–931. <http://dx.doi.org/10.1002/jqs.2582>.
- Yu, P.S., Mii, H.S., Murayama, M., Chen, M.T., 2008. Late Quaternary planktic foraminifer fauna and monsoon upwelling records from the western South China Sea, near Vietnam Margin (IMAGES MD012394). *Terr. Atmos. Ocean. Sci.* 19 (4), 347–362.
- Zhang, R., Delworth, T.L., 2005. Simulated tropical response to a substantial weakening of the Atlantic thermohaline circulation. *J. Clim.* 18, 1853–1860.